The American Journal of Pathology, Vol. 182, No. 4, April 2013

The American Journal of
PATHOLOGY
ajp.amjpathol.org

VASCULAR BIOLOGY, ATHEROSCLEROSIS, AND ENDOTHELIUM BIOLOGY

Targeting the IRE1α/XBP1 and ATF6 Arms of the Unfolded Protein Response Enhances VEGF Blockade to Prevent Retinal and Choroidal Neovascularization

Li Liu,* Xiaoping Qi,† Zhijuan Chen,† Lynn Shaw,* Jun Cai,† Layton H. Smith,‡ Maria B. Grant,* and Michael E. Boulton†

From the Departments of Pharmacology and Therapeutics and Anatomy and Cell Biology,† University of Florida, Gainesville; and the Cardiovascular Pathobiology Program,‡ Sandford Burnham Medical Research Institute at Lake Nona, Orlando, Florida*

Accepted for publication December 31, 2012.

Address correspondence to Michael E. Boulton, Ph.D., Department of Anatomy and Cell Biology, University of Florida, 1600 SW Archer Rd, PO Box 100235, Gainesville, FL 32610. E-mail: meboulton@ufl.edu.

Although anti-vascular endothelial growth factor (VEGF) treatments reduce pathological neovascularization in the eye and in tumors, the regression is often not sustainable or is incomplete. We investigated whether vascular endothelial cells circumvent anti-VEGF therapies by activating the unfolded protein response (UPR) to override the classic extracellular VEGF pathway. Exposure of endothelial cells to VEGF, high glucose, or H_2O_2 up-regulated the X-box binding protein-1/inositol-requiring protein-1 (IRE1) α and activating transcription factor 6 (ATF6) arms of the UPR compared with untreated cells. This was associated with increased expression in α-basic crystallin (CRYAB), which has previously bound VEGF. siRNA knockdown or pharmacological blockade of IRE1α, ATF6, or CRYAB increased intracellular VEGF degradation and decreased full-length intracellular VEGF. Inhibition of IRE1α, ATF6, or CRYAB resulted in an approximately 40% reduction of *in vitro* angiogenesis, which was further reduced in combination with a neutralizing antibody against extracellular VEGF. Blockade of IRE1α or ATF6 in the oxygen-induced retinopathy or choroidal neovascularization mouse models caused an approximately 35% reduction in angiogenesis. However, combination therapy of VEGF neutralizing antibody with UPR inhibitors or siRNAs reduced retinal/choroidal neovascularization by a further 25% to 40%, and this inhibition was significantly greater than either treatment alone. In conclusion, activation of the UPR sustains angiogenesis by preventing degradation of intracellular VEGF. The IRE1α/ATF6 arms of the UPR offer a potential therapeutic target in the treatment of pathological angiogenesis. *(Am J Pathol 2013, 182: 1412–1424; http://dx.doi.org/10.1016/j.ajpath.2012.12.020)*

It is evident that there exists a plethora of pro- and anti-angiogenic factors that regulate the ocular vasculature and influence the development and progression of aberrant neovascularization, such as in diabetic retinopathy and age-related macular degeneration (AMD). Furthermore, the spatiotemporal balance of these pro- and anti-angiogenic factors is critical in determining whether vascular homeostasis or a pathological condition predominates. The collective evidence suggests that the vascular endothelial growth factor (VEGF) family is critical for ocular angiogenesis,[1] and treatment of patients with AMD who have choroidal neovascularization (CNV) using inhibitors of extracellular VEGF, such as ranibizumab (Lucentis) or bevacizumab (Avastin), significantly reduces CNV.[2,3] However, as shown by the ANCHOR, MARINA, and VISION clinical trials, regression is often not sustainable or is incomplete and only approximately 50% of patients benefit significantly from this therapeutic strategy.[4,5] Furthermore, similar limitations are associated with the use of these anti-VEGF agents in treatment of proliferative diabetic retinopathy and diabetic macular edema.[6] The challenge, therefore, is to find an adjunct to the current therapy that will obviate the repeated injections, lower the dose of exogenous VEGF blocker, and act synergistically to elicit complete regression of the vascular lesion. There is increasing evidence from the cancer field that endothelial cells protect themselves and sustain tumor angiogenesis by intracellular accumulation of VEGF and self-regulation through an intracellular pathway.[7,8]

Supported by the James & Esther King Biomedical Foundation and NIH grant EY018358 (M.E.B.); NIH grants EY012601, EY007739, DK096221, and HL10170 (M.B.G.); and Florida Department of Health grant 60-NIR-09 (L.H.S.).

L.L. and X.Q. contributed equally to this work.

http://dx.doi.org/10.1016/j.ajpath.2012.12.020

Endoplasmic reticulum (ER) stress and the unfolded protein response (UPR)[9,10] play a critical role in transcriptional regulation of VEGF-A[11] and protect VEGF from intracellular degradation.[12] ER stress can activate one or more of the three ER stress sensors [protein kinase RNA-like endoplasmic reticulum kinase (PERK), inositol-requiring protein-1 (IRE1), and activating transcription factor 6 (ATF6)], leading to activation of the UPR pathway and production of chaperone proteins.[9,10] α-Basic crystallin (CRYAB) is a classic small heat shock protein that is up-regulated by ER stress and has interactive sequences for VEGF.[13] A strong association between CRYAB expression and angiogenesis has been shown. By using *CRYAB*$^{-/-}$ mice, Kase et al[14] reported an attenuation of CNV. Dimberg et al[15] showed that tumors in *CRYAB*$^{-/-}$ mice are significantly less vascularized than in wild-type mice. Based on these observations, we assessed whether activation of the UPR and downstream CRYAB up-regulation may sustain the VEGF signaling pathway and if targeting both extracellular VEGF and the UPR will represent a more effective strategy than current extracellular VEGF therapies alone.

Materials and Methods

Cell Culture

Bovine retinal microvascular endothelial cells were isolated and cultured, as previously described.[16] Briefly, freshly isolated bovine retinas were homogenized, and after trapping on an 83-μm nylon mesh, they were transferred into an enzyme mixture [500 μg/mL collagenase, 200 μg/mL protease (Pronase), and DNase] at 37°C for 20 minutes. The resultant vessel fragments were trapped on a 53-μm mesh, washed, and pelleted, and cells were plated in endothelial cell basal medium with growth supplement (Invitrogen, Carlsbad, CA) at 37°C, 5% CO_2, for 3 days. The cells were used within three passages.

Activation of the UPR

Retinal microvascular endothelial cells were treated with 100 ng/mL VEGF, 25 mmol/L glucose, or 200 μmol/L H_2O_2 for 24 hours. The 5.2 mmol/L medium alone acted as the baseline control because 5.2 mmol/L glucose is considered the normoglycemic control for cultured endothelial cells and hyperglycemia is usually in the range from 15 to 30 mmol/L glucose. We chose to use 25 mmol/L glucose based on our previous studies and 25 mmol/L mannitol as an osmotic control.[17] The expression levels of X-box binding protein (XBP)-1, ATF6, IRE1, PERK, CRYAB, and α-tubulin were determined by using Western blot analysis.

VEGF ELISA Measurement

Retinal endothelial cells were cultured in 6-well plates. After 24-hour treatment with 100 ng/mL VEGF, 25 mmol/L glucose, or 200 μmol/L H_2O_2, the cells were rinsed in PBS, and fresh microvascular endothelial basal medium with 5% fetal calf serum was added. After a further 24 hours, the culture medium was removed and centrifuged at 2000 × *g* for 10 minutes to remove cellular debris. The cell numbers of each well were counted before preparing total cell lysates using radioimmunoprecipitation assay (RIPA) buffer. VEGF concentrations were measured in duplicate in each sample from at least three separate experiments with a VEGF DuoSet enzyme-linked immunosorbent assay (ELISA; R&D Systems, Minneapolis, MN), according to the manufacturer's instructions. The results are expressed as ng/10^6 cells per day VEGF.

In Vitro LD_{50} of Potential Pharmacological UPR Inhibitors

We selected a list of compounds reported to be capable of inhibiting different UPR pathways (Table 1) and then measured their cytotoxicity using cultured retinal microvascular endothelial cells. In brief, cells were exposed to a serial dilution of test compound for 24 hours, and cytotoxicity was determined using the Cytotoxicity Detection Kit (Roche Applied Science, Indianapolis, IN), according to the manufacturer's instructions. This kit can detect lactate dehydrogenase activity released from damaged cells, and results are presented as the LD_{50}. Vehicle was used as a baseline control.

siRNA Knockdown of UPR Pathways in Cultured Endothelial Cells

Two siRNAs were synthesized by Life Technologies Corporation (Carlsbad, CA) against each of bovine CRYAB, IRE-1, ATF6, and PERK. The siRNA sequences are shown in Table 2. Scrambled siRNA acted as a negative control. Bovine microvascular endothelial cells were seeded in 6-well tissue culture dishes for 24 hours before transfection with respective siRNA (30 nmol/L) using siPORT transfection agent (Life Technologies Corporation, Carlsbad, CA) per the manufacturer instructions. Knockdown was confirmed by Western blot analysis.

Western Blot Analysis and Immunoprecipitation

Western blot analysis and immunoprecipitation were performed as previously described.[18] In brief, cells were

Table 1 LD_{50} of Compounds That Inhibit UPR Proteins in Bovine Microvascular Endothelial Cells

Compounds	ID_{50} (μmol/L)	UPR proteins
MG132	75	IRE1α/XBP-1
17-AAG	2	IRE1α
1-NM-PP1	50	IRE1α
AEBSF	1500	ATF6
Lactacystin	35	IRE1α/XBP-1

AEBSF, 4-(2-aminoethyl) benzenesulfonyl fluoride hydrochloride.

Table 2 Corresponding *Silencer* siRNA Construction Kit Template Sequences

siRNA	Sense primer	Antisense primer
IRE1	5′-AAGTACCAAATGTCCTGCTTTCCTGTCTC-3′	5′-AAAAAGCAGGACATTTGGTACCCTGTCTC-3′
IRE1	5′-AAATGGCGATCATCTTCTCTACCTGTCTC-3′	5′-AATAGAGAAGATGATCGCCATCCTGTCTC-3′
ATF6	5′-AAAGTCACGGAAAGTTTTCCACCTGTCTC-3′	5′-AATGGAAAACTTTCCGTGACTCCTGTCTC-3′
ATF6	5′-AATCACTCGACCTCCCAACTTCCTGTCTC-3′	5′-AAAAGTTGGGAGGTCGAGTGACCTGTCTC-3′
PERK	5′-AATGCCTTCGATGTTGTTGTACCTGTCTC-3′	5′-AATACAACAACATCGAAGGCACCTGTCTC-3′
PERK	5′-AACATTGAAGACACCCCTCTTCCTGTCTC-3′	5′-AAAAGAGGGGTGTCTTCAATGCCTGTCTC-3′
CRYAB	5′-AAATCCTGGCGCTCTTCATGTCCTGTCTC-3′	5′-AAACATGAAGAGCGCCAGGATCCTGTCTC-3′
CRYAB	5′-AAGAATCCGTCAGCTTCAGCACCTGTCTC-3′	5′-AATGCTGAAGCTGACGGATTCCCTGTCTC-3′

Silencer siRNA construction kit (part No. AM1620; Life Technologies Corporation, Carlsbad, CA).

washed with PBS and lysed in RIPA buffer at 4°C containing a cocktail of protease (Sigma-Aldrich, St. Louis, MO) and phosphatase (Roche Applied Science) inhibitors for 30 minutes. Lysates were centrifuged, supernatants were collected, and total protein concentration was determined by the MicroBCA reagent assay (Pierce, Rockford, IL). Western blot analysis was performed after SDS-PAGE (10% gel; equal aliquot of total proteins per lane) and transfer onto polyvinylidene difluoride membranes. The IRE1α, ATF6, CRYAB, and VEGF proteins were detected using an affinity-purified rabbit or mouse anti-IRE1α (Sigma-Aldrich), anti-ATF6 (Sigma-Aldrich), anti-CRYAB (Novus Biologicals, LLC, Littleton, CO), and anti-VEGF (Sigma-Aldrich), followed by incubation with polyclonal anti-rabbit in goat or mouse in rabbit horseradish peroxidase–conjugated secondary antibodies (Sigma-Aldrich) at 1:2000 dilution. The proteins were detected and visualized with the ECL Plus Western Blotting Detection System (GE Healthcare Biosciences, Pittsburgh, PA), and resultant bands were normalized against α-tubulin (Sigma-Aldrich). The intensity of each immunoreactive band was quantified using ImageJ software version 1.46 (NIH, Bethesda, MD).[18] For immunoprecipitation, total proteins were immunoprecipitated with 10 μg of relevant antibodies for 2.5 hours at 4°C, followed by the addition of 20 μL of protein A/G-agarose overnight at 4°C. The resultant pellet was dissolved in 2× Laemmli buffer (Bio-Rad Laboratories, Hercules, CA) and subjected to Western blot analysis.

In Vitro Tube Formation Assay

In vitro tube formation assays were performed as previously described.[16] Briefly, near-confluent microvascular endothelial cells were pretreated with 100 ng/mL VEGF for 2 hours and then either treated for 24 hours with test compounds at serial concentrations, as indicated, or VEGF165 neutralizing antibody or washed and maintained in basal medium for 24 hours to establish the intracrine VEGF signaling pathway, before treatment with test compounds or VEGF165 neutralizing antibody (anti-human VEGF165, AB-293-NA; R&D Systems), which we have previously shown to bind strongly to bovine VEGF. Cells without VEGF treatment or with VEGF only were used as control. In addition, siRNA-treated cells, with or without VEGF, were also assessed. The cells were then detached and plated at the concentration of 2.5×10^4 per well on 24-well plates coated with 12.5% (v/v) growth factor–poor Matrigel (BD, Franklin Lakes, NJ) and left overnight. The medium was then aspirated, and 250 μL per well of 12.5% Matrigel was overlaid on the cells for 2 hours to allow the polymerization of Matrigel, followed by the addition of 500 μL per well of basal medium, MCD131, with 10% fetal calf serum for 24 hours. The following day, the culture plates were observed under a phase-contrast microscope and imaged using five random fields (original magnification, ×10). The tubule length (mm/mm^2) per microscope field was quantified.

VEGF Degradation

VEGF degradation was assessed as previously described.[12] Briefly, the cells were trypsinized and pelleted at $2000 \times g$ for 5 minutes. The resultant pellets were dissolved in 500 μL of denaturing buffer (20 mmol/L Tris-HCl, pH 8.0, 6 mol/L guanidine-HCl, 5 mmol/L EDTA, and 4 mmol/L dithiothreitol) at room temperature for 2 hours. Total protein concentration was estimated by measuring the UV absorbance at 280 nm and diluted with denaturing buffer to a final concentration of 1 mg/mL. After centrifugation at $46{,}000 \times g$ at 4°C for 30 minutes, the supernatant was concentrated to 100 μL using Millipore Ultrafree centrifugal devices (molecular weight cutoff, 3.5 kDa) (Millipore, Bedford, MA). The samples were mixed with 1:2 standard sample buffer and analyzed by using Western blot analysis using an antibody against the C-terminal of human VEGF (Abcam, Cambridge, MA). In accordance with previous studies, the degradation of VEGF resulted in multiple lower molecular weight bands, of which a fragment of approximately 38 kDa is prominent.[19]

Animal Studies

All mice were housed under specific pathogen-free conditions and handled in accordance with the Association for Research in Vision and Ophthalmology statement for Use of Animals in Ophthalmic and Vision Research and the guidelines of the Institutional Animal Care and Use Committee at the University of Florida (Gainesville, FL). Two animal models were used; the oxygen-induced retinopathy (OIR) model, which is representative of retinal neovascularization, as occurs in retinopathy of prematurity and diabetic retinopathy,

and the laser-induced CNV model, which is representative of aberrant vascular growth in AMD.

OIR Model

For the OIR model, C57BL/6 mouse pups were exposed to 75% oxygen from postnatal day 7 (P7) to P12, along with nursing mothers.[20] On day P12, the pups were removed from high oxygen conditions, and on P17, mice were sacrificed. Eyes were fixed in paraformaldehyde, paraffin embedding was performed, and serial sections (5 μm thick) were obtained. Representative sections (every 30th section) across the retina were stained with H&E to visualize retinal structure and note any overt toxicity. A masked investigator counted all endothelial cell nuclei above the internal limiting membrane in all representative sections through each eye. Vascular cell nuclei are considered to be associated with neovascularization if they are on the vitreous side of the internal limiting membrane and the region of the optic nerve is not considered. The data presented represent random sampling from a minimum of 12 pups per treatment group. Efficacy of treatment was calculated as the percentage average nuclei per section in the eyes treated with test agent compared with vehicle control.

CNV Model

The laser procedure was undertaken as previously described.[21] Briefly, 8-week-old female C57BL/6 mice were anesthetized with a mixture of 80 mg/kg ketamine and 10 mg/kg xylazine, and their pupils were dilated with 0.5% tropicamide and 2.5% phenylephrine. Under the fundus microscope, an argon green ophthalmic laser, coupled to a slit lamp set to deliver a 50-millisecond pulse at 200 mW, with a 50-μm spot size, was used to rupture the Bruch's membrane in three quadrants of the right eye, located approximately 50 mm from the optic disk at relative positions of 9 AM, 12 PM, and 3 PM. The left eye served as an untreated control. Mice were sacrificed 14 days after laser injury, and the eyes were enucleated. For measuring lesion volume, we used a vascular-specific dye, Ricinus Communis Agglutinin I conjugated to rhodamine, to label whole flat mounts of retinal pigment epithelium (RPE)/choroid/sclera. The laser lesions were then imaged by Z-series laser scanning confocal microscopy to obtain lesion volume using ImageJ software version 1.46. In all CNV studies, animals were randomized and treatments were blinded until all analysis was complete. All determinations were performed in at least six animals per group. In addition, gross retinal/choroidal structure and vascular patterns were examined for possible adverse effects of the test compound or vehicle.

Treatment Regimen

Mice received an intravitreal injection in the left eye of 0.5 μL in the OIR model and 1.0 μL in the CNV model while the right eye acted as the uninjected control. Groups of six animals received the following treatments.

siRNA Treatment

Ambion *in Vivo* siRNAs predesigned and prevalidated for targeting murine CRYAB (s64457), IRE1 (s95857), ATF6 (s105469), and scrambled were purchased from Life Technologies Corporation. These siRNAs incorporated additional chemical modifications for superior serum stability with *in vivo* applications and reduced susceptibility to degradation by ribonucleases. All siRNAs were 19mer to avoid the potential anti-angiogenic effect of 21mer or longer siRNAs acting via toll-like receptor 3.[22] As previously determined, 1 and 2 μg per eye siRNA was delivered intravitreally at P12 in the OIR model or the time of laser injury in the CNV model.

UPR Pathway Inhibitor Treatment

A total of 5 μmol/L of potential UPR pathway inhibitor, MG132, and 50 μmol/L 4-(2-Aminoethyl) benzenesulfonyl fluoride hydrochloride (AEBSF) were delivered intravitreally at P12 in the OIR model or the time of laser injury in the CNV model. Saline or dimethyl sulfoxide vehicle controls were also included.

VEGF164 Neutralizing Antibody Treatment

A total of 5 ng per eye VEGF164 neutralizing antibody (anti-mouse VEGF164, AF-493-NA; R&D Systems) was delivered intravitreally at P12 in the OIR model or the time of laser injury in the CNV model. In some studies, the antibody was also given at 7 days after laser injury. Vehicle and 5 ng per eye of the appropriate Fc fragment (Jackson Immunoresearch, West Grove, PA) were included as controls.

Combined Treatment

For combination therapy, 5 ng per eye of VEGF164 neutralizing antibody was delivered intravitreally, together with siRNA or UPR inhibitor at P12 in the OIR model or the time of laser injury in the CNV model. In some studies, the antibody was also given at 7 days after laser injury.

Confirmation of siRNA Knockdown

For PCR assessment, 6-week-old female C57BL/6J mice received an intravitreal injection of 2 μg/μL siRNA at laser injury in the CNV model into the left eye, whereas the right eye served as an uninjected control. All siRNAs were as previously described. Mice were sacrificed at 2 days after treatment, eyes were enucleated, and the retina plus RPE/choroid were isolated. Total RNA was extracted with TRIzol total RNA isolation reagent (Invitrogen) and quantified using a Nanodrop Spectrophotometer (NanoDrop Products, Wilmington, DE). cDNA was synthesized from 1 μg total RNA from each sample using the iScript cDNA Synthesis Kit (Bio-Rad, Hercules, CA). cDNA at 1:10 dilution was used for quantitative RT-PCR (RT-qPCR) on a BioRad C1000 Thermal Cycler. mRNA expression was assessed using the RT^2 qPCR Primer Assay from Qiagen (Valencia, CA), with the following primers: mouse Ern1 (PPM36937A-200), mouse Cryab (PPM03570F-200), and mouse Atf6 (PPM33057A-200).

Final expression was normalized to the housekeeping gene, glyceraldehyde-3-phosphate dehydrogenase (GAPDH): RT[2] qPCR Primer Assay for mouse GAPDH (PPM02946E-200). Relative transcript abundance was determined by using the $\Delta\Delta C_T$ or ΔC_T method after normalization with GAPDH. All samples were run in triplicate. Error bars represent SEM.

For immunohistochemistry (IHC), 6-week-old female C57BL/6J mice received an intravitreal injection of 2 μg/μL siRNA at laser injury and were sacrificed at 14 days after treatment. Eyes were enucleated, and the RPE/choroid/sclera were prepared and then blocked with 10% normal goat sera, plus 1% bovine serum albumin for 2 hours at room temperature. Mouse monoclonal anti-CRYAB, anti-ATF6, and rabbit polyclonal anti-IRE1 (Lifespan Biosciences, Seattle, WA) were diluted 1:50 and 1:200, respectively, in PBS with 1% normal goat sera plus 1% bovine serum albumin and incubated overnight at 4°C. Tissues received a secondary antibody conjugated with fluorescein isothiocyanate in 1:600 for 1 hour at room temperature in the dark. To visualize vessels, we used a vascular-specific dye, Ricinus Communis Agglutinin I, conjugated to tetramethylrhodamine isothiocyanate (TRITC), to label the whole flat mounts of RPE/choroid, which were incubated for 30 minutes at room temperature in 1:400 of 10 mmol/L HEPES, 150 mmol/L NaCl, and 0.1% Tween 20. The tissues were covered in aqueous VectaShield mounting medium (Vector Laboratories, Inc., Burlingame, CA) for observation on an Olympus DSU-Olympus IX81 confocal microscope (Olympus America, Inc., Center Valley, PA).

Statistical Analysis

All experiments were repeated at least three times. Results are expressed as means ± SEM. The Mann-Whitney test was used to determine statistical significance of the densitometry data of Western blot analysis. An unpaired two-tailed Student's *t*-test was performed for the significance of the results of ELISA, *in vitro* tubule formation assay, *in vivo* CNV, and OIR models. Statistical analysis was performed using Prism 5 version 5.01 (GraphPad Software, Inc., La Jolla, CA) with $P < 0.05$ considered statistically significant.

Results

Induction of ER Stress and CRYAB Up-Regulation

It has previously been reported that growth factors, hyperglycemia, and oxidative stress can activate the ER stress response.[9,10] Western blot analysis demonstrated that exposure

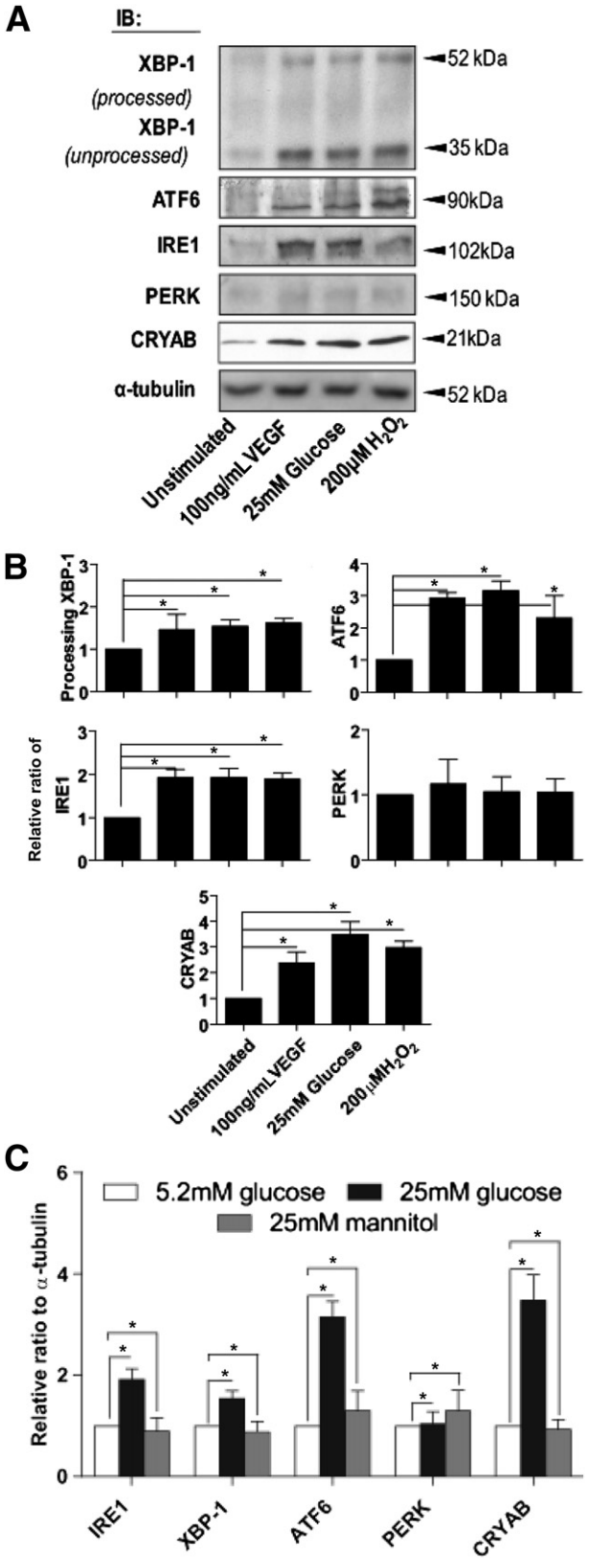

Figure 1 The effect of cellular stress on the UPR pathways and CRYAB expression. Confluent retinal microvascular endothelial cells were treated with 100 ng/mL VEGF, 25 mmol/L glucose, or 200 μmol/L H_2O_2 for 24 hours. Cells treated with 5.2 mmol/L glucose containing medium alone acted as a negative control (unstimulated). Cell lysates were prepared in RIPA buffer, and samples were assessed by using Western blot analysis for XBP-1 (processed and unprocessed), ATF6, IRE1α, PERK, and CRYAB. α-Tubulin served as the loading control. **A:** Representative Western blot analysis. **B:** Quantitation of Western blot analyses from a minimum of three separate experiments presented as the relative ratio to the tubulin loading control. **C:** Comparison of ATF6, IRE1α, XBP-1, PERK, and CRYAB protein expression in cells exposed to 25 mmol/L glucose or 25 mmol/L mannitol, determined by quantitation of Western blot analyses from a minimum of three separate experiments presented as the relative ratio of CRYAB to the tubulin loading control. $^*P < 0.05$.

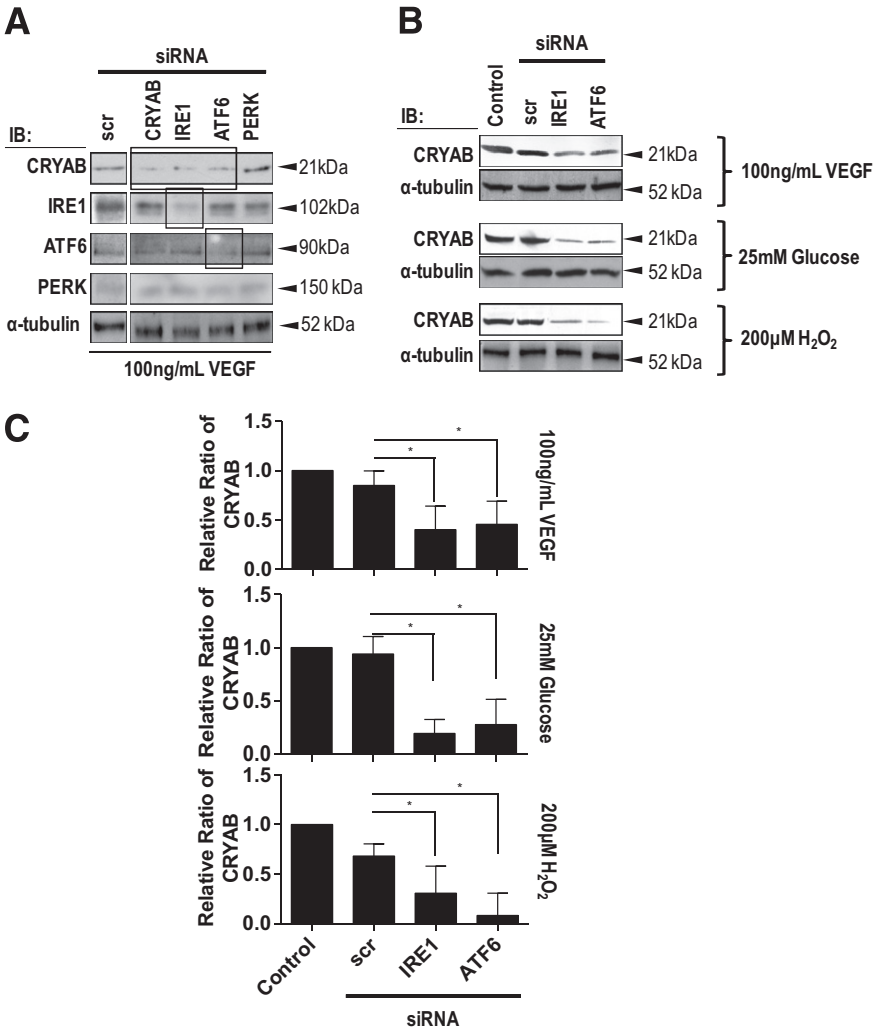

Figure 2 The effect of siRNA knockdown of the UPR pathways on CRYAB expression. Confluent retinal microvascular endothelial cells were treated with 100 ng/mL VEGF, 25 mmol/L glucose, or 200 μmol/L H_2O_2 for 24 hours in the presence of 30 nmol/L IRE1α, ATF6, or PERK siRNA. Cells treated with 5.2 mmol/L glucose containing medium alone or exposed to scrambled siRNA (scr) acted as negative controls. Cell lysates were prepared in RIPA buffer, and samples were assessed by using Western blot analysis for XBP-1 (processed and unprocessed), ATF6, IRE1α, PERK, and CRYAB. α-Tubulin served as the loading control. **A**: Confirmation that siRNA treatment resulted in the knockdown of CRYAB, IRE1α, ATF6, or PERK. **B**: Representative Western blot analysis. **C**: Quantitation of Western blot analyses from a minimum of three separate experiments presented as the relative ratio to the tubulin loading control. Comparison of CRYAB protein expression in cells exposed to 25 mmol/L glucose or 25 mmol/L mannitol, determined by quantitation of Western blots from a minimum of three separate experiments presented as the relative ratio of CRYAB to the tubulin loading control. $*P < 0.05$. IB, immunoblot.

of microvascular endothelial cells to VEGF, high glucose, or H_2O_2 caused an up-regulation of the XBP-1/IRE1α and ATF6 arms of the UPR; however, no effect was observed on PERK when compared with untreated control cells (Figure 1, A and B). A total of 25 mmol/L mannitol, used as an osmotic control for 25 mmol/L glucose, showed no significant change compared with 5.2 mmol/L glucose containing normoglycemic control medium (Figure 1C). Activation of IRE1 by ER stress generates a mature *XBP-1* mRNA by unconventional splicing of *XBP-1* pre-mRNA,[9] and activated XBP-1 up-regulates molecular chaperone genes, including CRYAB. All three UPR stressors resulted in a significant increase in CRYAB expression compared with control (Figure 1, A and B). siRNA knockdown of IRE1α, ATF6, PERK, or CRYAB significantly reduced the expression of their respective proteins (Figure 2A). siRNA knockdown of IRE1α or ATF6 both caused a significant reduction in VEGF-, high glucose−, or H_2O_2-induced CRYAB expression compared with untreated controls or those receiving scrambled siRNA (Figure 2, B and C), indicating that these two arms of the UPR pathway are participating in maintaining homeostasis of ER stress. A total of 25 mmol/L mannitol was used as an osmotic control for 25 mmol/L glucose and showed no significant change compared with 5.2 mmol/L glucose-containing normoglycemic control medium (data not shown). PERK knockdown had no effect on CRYAB expression (Figure 2, B and C).

Induction of ER Stress Inhibits Intracellular VEGF Degradation and Leads to VEGF Accumulation

To verify our hypothesis that ER stress, and subsequent up-regulation of CRYAB, prevented VEGF degradation, we undertook Western blot analysis on cell lysates to assess intracellular VEGF and the extent of its degradation. Exposure to VEGF, high glucose, or H_2O_2 resulted in a large increase in secreted VEGF, which was much greater than intracellular VEGF levels (Figure 3A). In contrast, only VEGF or high glucose led to a significant increase in intracellular VEGF, which presented as a 42-kDa band by using Western blot analysis (Figure 3B). A total of 25 mmol/L mannitol, used as an osmotic control for 25 mmol/L glucose, showed no significant change compared with 5.2 mmol/L glucose containing normoglycemic control medium (Figure 3A). siRNA-mediated knockdown of

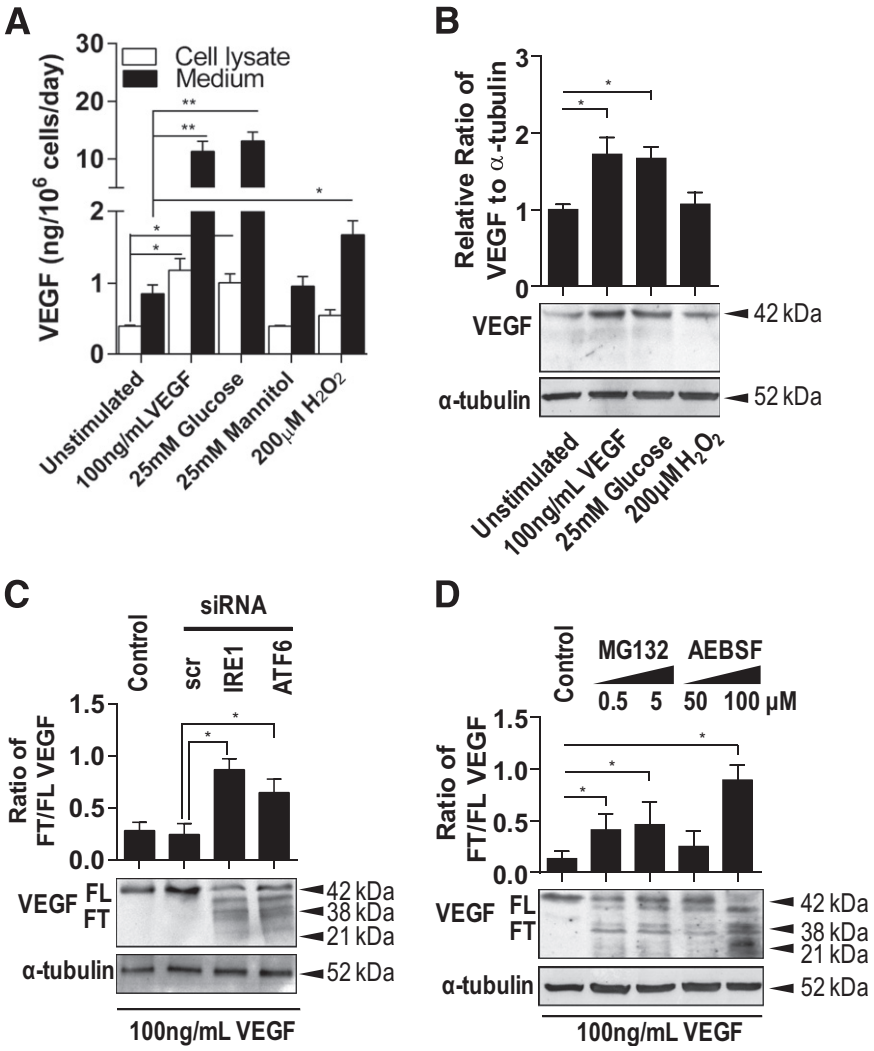

Figure 3 The effect of ER stress induction on VEGF expression and intracellular VEGF degradation. Confluent bovine retinal microvascular endothelial cell cultures were treated with 100 ng/mL VEGF, 25 mmol/L glucose, or 200 μmol/L H_2O_2 for 24 hours. Cells treated with 5.2 mmol/L glucose containing medium alone or medium supplemented with 25 mmol/L mannitol acted as negative controls. **A**: VEGF expression in the culture medium and cell lysates was measured by ELISA. **B**: The overall VEGF protein levels in cell lysates were determined by using Western blot analysis. When VEGF was the stressor, cells were rinsed with PBS to remove exogenous VEGF and then incubated for a further 24 hours. **C**: Cultures were transfected with siRNA directed against IRE1α or ATF6, or scrambled siRNA (scr), for 24 hours, and the cells were then treated with 100 ng/mL VEGF for 24 hours. The total cellular proteins were subjected to Western blot analysis to determine the relative ratio of full-length (FL) VEGF to VEGF fragments (FT). **D**: Retinal endothelial cells were treated with different concentrations of MG132 or AEBSF, as indicated in the presence of 100 ng/mL VEGF for 24 hours. The total cellular proteins were subjected to Western blot analysis to determine the relative ratio of FL VEGF to VEGF fragments. α-Tubulin served as the loading control. Quantitation is from a minimum of three experiments, and the results from representative Western blot analyses are shown. $*P < 0.05$, $**P < 0.01$. The error bars show SEM.

either IRE1α or ATF6 expression in cells exposed to exogenous VEGF resulted in a decrease in total full-length intracellular VEGF and the appearance of VEGF fragments, with a range of molecular weights compared with scrambled siRNA control in which only full-length VEGF was observed (Figure 3C). We next tested two putative IRE1α inhibitors, MG132 and AEBSF.[23,24] The cytotoxicity of these compounds on retinal endothelial cells was assessed with the Cytotoxicity Detection Kit (Roche Applied Science), and no significant toxicity was detected at any of the concentrations used in this study (Table 1). Both compounds significantly increased the fragmentation of VEGF in a dose-dependent manner compared with untreated controls (Figure 3D).

Inhibition of the IRE1α or ATF6 Pathways of the UPR Partially Inhibits VEGF-Induced *in Vitro* Angiogenesis

We hypothesized that inhibition of the UPR pathways or the downstream effector, CRYAB, would reduce intracellular VEGF and, thus, partially reduce VEGF-induced angiogenesis. siRNA knockdown of IRE1α, ATF6, or CRYAB resulted in a maximal reduction of approximately 40% in tubule formation compared with VEGF-stimulated control or cells treated with scrambled siRNA (Figure 4, A and B). MG132 resulted in a dose-dependent reduction in tubule formation of approximately 75% compared with VEGF-stimulated control or cells treated with scrambled siRNA (Figure 4, A and C). AEBSF also showed partial inhibition of tubule formation of approximately 30%, which was similar at all concentrations tested (Figure 4, A and D).

Blocking Both the UPR Pathway and Extracellular VEGF Has an Additive Effect on the Inhibition of *in Vitro* Angiogenesis

Next, we determined if combined inhibition of extracellular VEGF and the UPR pathway was more effective in preventing *in vitro* angiogenesis than either treatment alone. As anticipated, anti-VEGF antibody prevented the immediate angiogenic effect of exogenous VEGF, whereas the UPR inhibitors had minimal or no effect on tubule formation

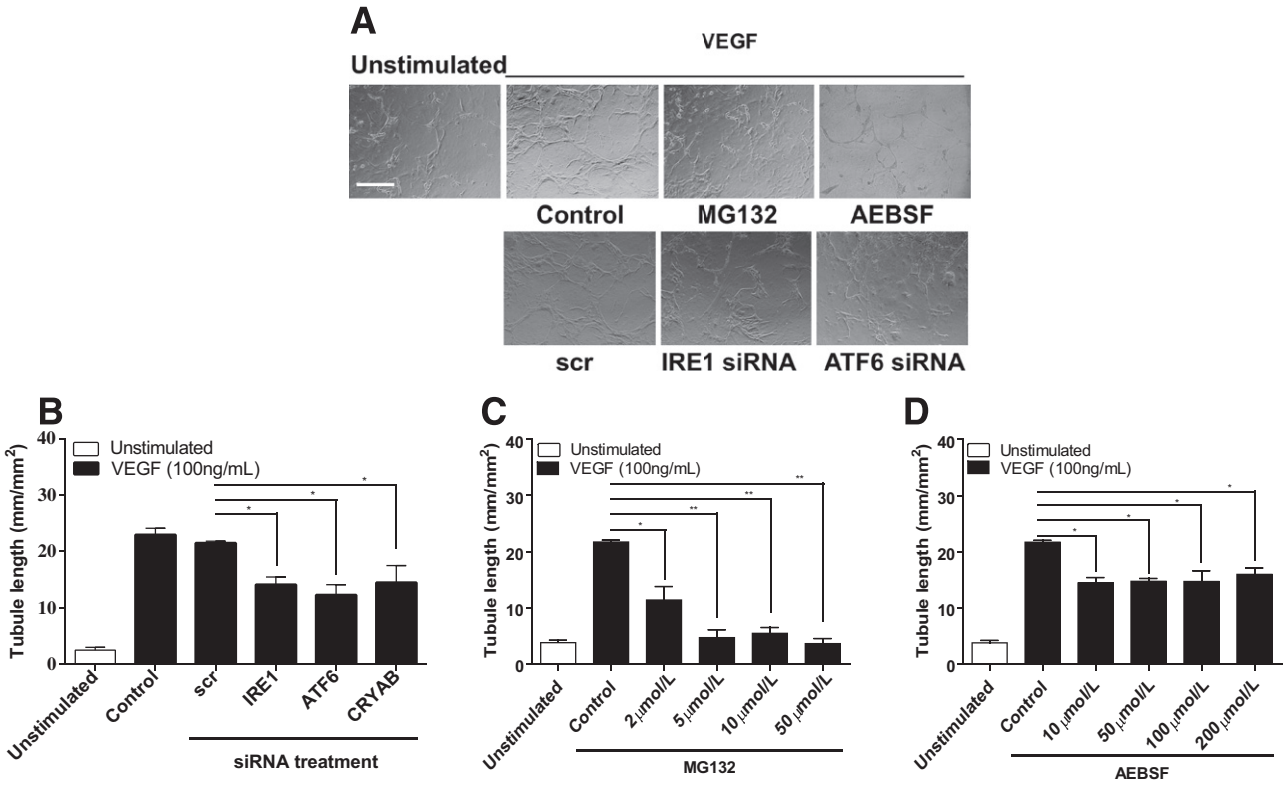

Figure 4 The effect of inhibiting the IRE1α or ATF6 pathways of the UPR on VEGF-induced *in vitro* angiogenesis. Retinal endothelial cells were seeded between two layers of Matrigel in the presence or the absence of 100 ng/mL VEGF for 48 hours. Morphometric analysis of *in vitro* tubule length (mm/mm^2) per microscope field was performed. **A:** Representative photomicrographs of tubule formation in the presence or the absence of 100 ng/mL VEGF with siRNAs directed against IRE1α or ATF6, MG132, or AEBSF. Medium alone or cells transfected with scrambled siRNA (scr) acted as control. Images were taken 24 hours later. **B:** Subconfluent cells were transfected with siRNAs directed against IRE1, ATF6, or CRYAB for 24 hours before the *in vitro* tubule formation assay. **C:** Cells were treated with different concentrations of MG132, as indicated for 24 hours before the *in vitro* tubule formation assay. **D:** Cells were treated with different concentrations of AEBSF, as indicated for 24 hours before the *in vitro* tubule formation assay. Each experiment was repeated a minimum of three times. $*P < 0.05$, $**P < 0.01$. The error bars show the SEM.

(Figure 5A). However, in cells that had received prior stimulation by VEGF, followed by either anti-VEGF antibody, MG132, or IRE1α siRNA 24 hours later showed a time-dependent reduction in tubule formation of approximately 40%, 60%, and approximately 75%, respectively (Figure 5B). By contrast, a combination of anti-VEGF using either MG132 or IRE1α siRNA resulted in 77% and 94% inhibition of tubule formation at 24 hours after exposure (Figure 5B).

Blocking Both the UPR Pathway and Extracellular VEGF Is More Effective Than Either Alone in Inhibiting Neovascularization in the Laser-Induced CNV and OIR Mouse Models of Angiogenesis

To confirm that siRNA against IRE1α, ATF6, or CRYAB resulted in knockdown of the respective proteins in mouse eyes, we undertook RT-qPCR and IHC (Figure 6, A and B). As can be seen in Figure 6A, siRNA knockdown resulted in

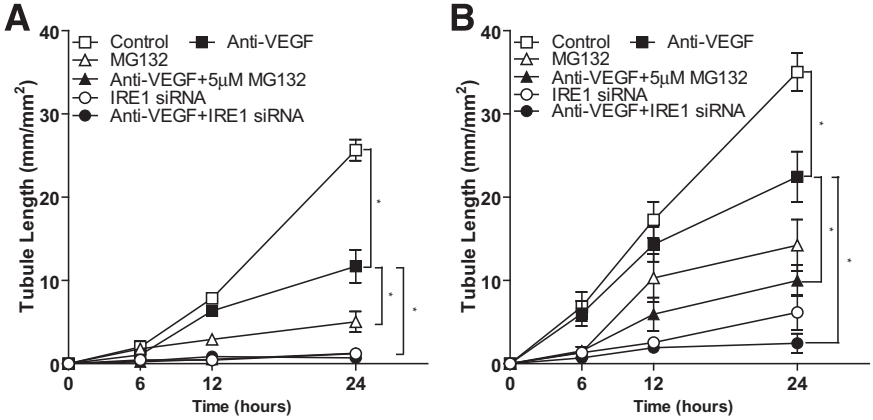

Figure 5 The effect of blocking both the UPR pathway and extracellular VEGF on *in vitro* angiogenesis. **A:** Endothelial cells were exposed to a combination of 100 ng/mL VEGF and a neutralizing antibody against VEGF, IRE1α siRNA, MG132, or a neutralizing antibody against VEGF in the presence of either IRE1α siRNA or MG132. **B:** Cells were pre-exposed to 100 ng/mL VEGF for 24 hours and then exposed to vehicle control, a neutralizing antibody against VEGF, IRE1α siRNA, MG132, or a neutralizing antibody against VEGF in the presence of IRE1α siRNA or MG132. After incubation, cells were transferred to Matrigel and tubule length (mm/mm^2) was measured 24 hours later. The data represent the means ± SEM from a minimum of three experiments. $*P < 0.05$.

a significant knockdown of CRYAB, ATF6, and IRE1 by 2 days after treatment in the neural retina/RPE/choroid by 65%, 57%, and 38%, respectively, compared with scrambled control. To confirm that knockdown of CRYAB, ATF6, and IRE1 was occurring in the vasculature, we used IHC. UPR proteins were strongly expressed in CNV lesions 14 days after laser injury, either untreated or receiving scrambled siRNA, and this was associated with both retinal vessels and surrounding tissues (Figure 6B). By contrast, only weak immunofluorescence staining for UPR proteins in CNV lesions was observed in mice receiving intravitreal siRNA, and there was minimal association with the vasculature in these lesions.

We next tested if inhibition of the IRE1α and ATF6 UPR pathways would inhibit angiogenesis *in vivo* and if combined inhibition was more effective than single pathway blockade. siRNA knockdown of IRE1α, ATF6, or CRYAB or application of pharmacological inhibitors by intravitreal injection all significantly reduced angiogenesis in the laser-induced CNV and OIR models by 40% to 60% (Figures 6 and 7). A total of 5 ng per eye intravitreal injection of anti-VEGF164 (based on a dose-response study, data not shown) resulted in a 30% to 40% inhibition of neovascularization in both models. Intravitreal injection of the Fc fragment showed no significant difference compared with the vehicle control (Figure 6, C and D). In both animal

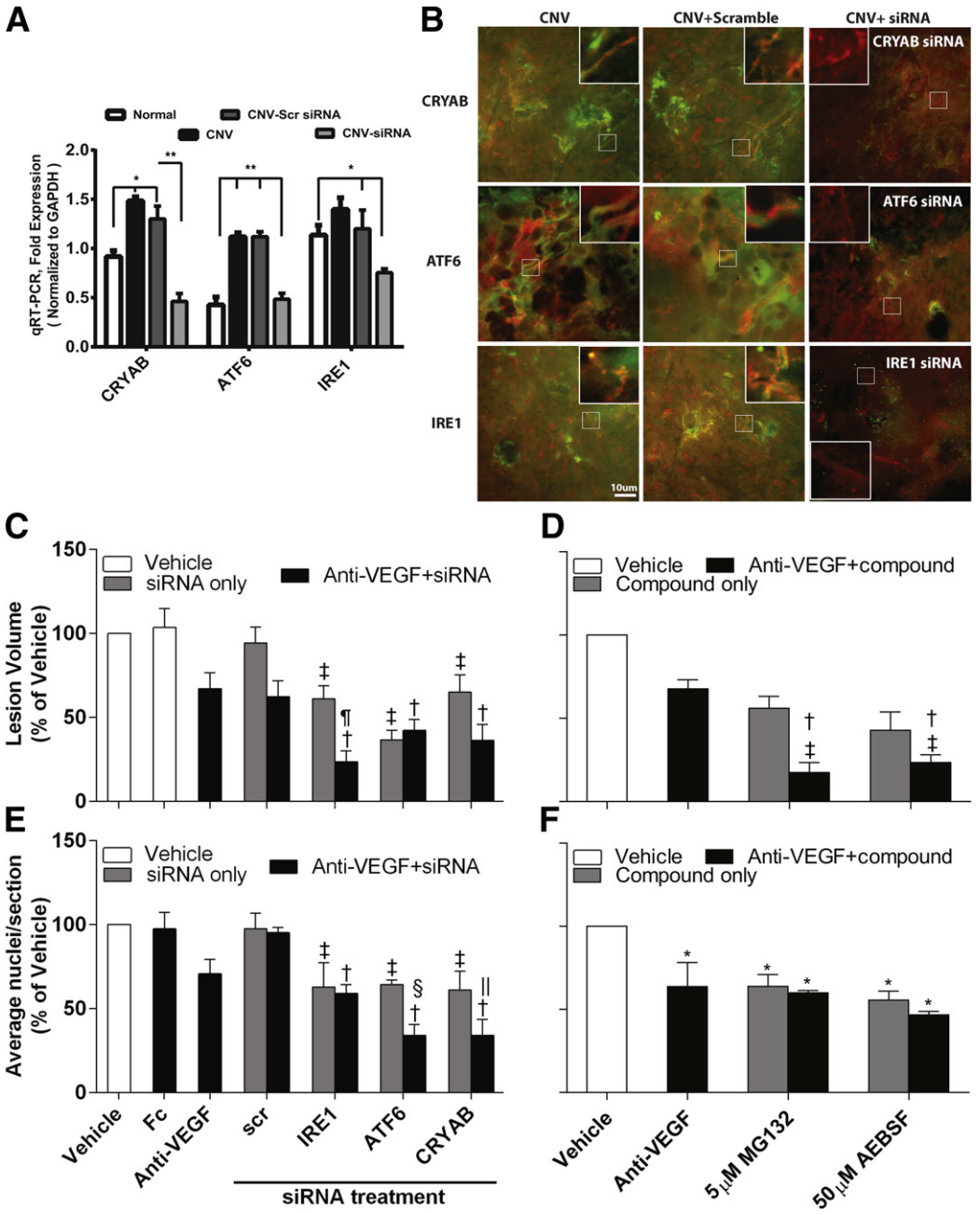

models, combined CRYAB siRNA and anti-VEGF treatment had a significantly greater inhibitory effect than either treatment alone and reduced angiogenesis by at least 60% (Figure 6, C and E, and Figure 7). Interestingly, different UPR pathways appear to be involved in the CNV and OIR models. IRE1α, but not ATF6, knockdown had an additive effect with anti-VEGF treatment in the CNV model, whereas ATF6, but not IRE1α, knockdown had an additive effect with anti-VEGF treatment in the OIR model (Figure 6, C and E). However, our interpretation is limited to only counting pre-inner limiting membrane nuclei in the OIR model, and we have not assessed the degree of vaso-obliteration or the area associated with neovascular tufts. Our observations were further supported by studies using the pharmacological inhibitors, MG132 and AEBSF, which predominantly target the IRE1α and ATF6 pathways of the UPR, respectively. Both agents had a significantly greater inhibitory effect when given with anti-VEGF than either agent alone in the CNV model and reduced angiogenesis by at least 70% (Figure 6, D and F, and Figure 7). By contrast, neither compound improved anti-VEGF strategies in the OIR model.

Discussion

In this study, we show the following: i) high glucose, oxidative stress, or VEGF causes ER stress and activation of the UPR pathway, which, in turn, increases CRYAB, ii) siRNA knockdown of IRE1α, XBP-1, ATF6, or CRYAB each increase VEGF degradation and reduce intracellular VEGF levels, iii) a decrease of XBP1/IRE1α, ATF6, or CRYAB inhibits *in vitro* angiogenesis and elicits a partial reduction in angiogenesis in both the CNV and OIR models, and iv) combination therapy blocking both the UPR and extracellular VEGF further reduces *in vitro* angiogenesis and retinal/choroidal neovascularization.

There is extensive literature reporting that ER stress and activation of the UPR are associated with pathological angiogenesis associated with diabetic complications, macular degeneration, and tumors.[25–29] There are a multitude of extrinsic and intrinsic factors that can initiate the ER stress response, leading to the accumulation of unfolded or misfolded proteins.[30,31] Interestingly, even exogenous VEGF can lead to an increase in unfolded/misfolded proteins in the ER and activation of the UPR.[32] The UPR pathway increases protein maturation machinery, including molecular chaperones, which are involved in the recognition, binding, solubility, and refolding of proteins. These unfolded/misfolded proteins interact with immunoglobulin binding protein BiP, causing its release from one or more of the three ER stress sensors, PERK, IRE1α, and ATF6, which leads to activation of the UPR pathway(s) and the production of chaperone proteins.[9,10] The small heat shock proteins compose a class of molecular chaperones that are characterized by their low molecular weight (12 to 34 kDa), a conserved C-terminal domain (the α-crystallin domain), and a helical N- and a short flexible C-terminus extension.[33] One such small heat shock protein [namely, CRYAB (HSPB5)] has been strongly implicated in angiogenesis. First, CRYAB is significantly increased in tumor vessels[12] and tumors grown in *CRYAB*$^{-/-}$ mice are significantly less vascularized than wild-type tumors.[15] Second, CRYAB expression is up-regulated in both diabetic retinopathy and CNV[34,35] and intraocular angiogenesis is attenuated in *CRYAB*$^{-/-}$ mice.[14] Third, CRYAB has interactive sequences for VEGF.[13]

Our study shows that high glucose, oxidative stress, and VEGF (all factors associated with pathological angiogenesis) activate the UPR and lead to increased expression of CRYAB. Based on siRNA knockdown, it appears that this is facilitated by the IRE1α and ATF6 arms of the UPR, but not the PERK. CRYAB is a soluble cytosolic protein that, in addition to its ability to act as a molecular chaperone that counteracts the formation of aberrantly folded polypeptides

Figure 6 The effect of blocking both the UPR pathway and extracellular VEGF on neovascularization in the laser-induced CNV and OIR mouse models of angiogenesis. **A** and **B**: Mice underwent the CNV model and received a 1-μL intravitreal injection of 2 μg per eye siRNAs against IRE1α, ATF6, or CRYAB (scrambled siRNA was used as a control), and animals were sacrificed at 2 days after laser injury for RT-qPCR or 14 days after laser injury for IHC. *$P < 0.05$, **$P < 0.01$. **A**: Eyes were enucleated, and the retina plus RPE/choroid were surgically isolated. Total RNA was extracted, and the expression of IRE1α, ATF6, or CRYAB was determined by RT-qPCR and normalized to the housekeeping gene, *GAPDH*. There were six mice per group. Error bars represent SEM. **B**: RPE/choroidal flat mounts were dual stained with a vascular-specific marker, agglutinin—tetrarhodamine isothiocyanate (TRITC) conjugate, to visualize the CNV vessels (red) and antibodies against CRYAB, ATF6, or IRE1, followed by a secondary antibody conjugated with fluorescein isothiocyanate (green). Representative confocal microscopy images are shown, in which orange indicates colocalization of vessels and the appropriate UPR protein. Higher-magnification images (**insets**) are provided to show changes in colocalization in the vasculature under different conditions. **C** and **D**: Mice underwent the CNV model, and animals were terminated at 14 days after laser injury. Lesions were labeled with vascular-specific dye, Ricinus Communis Agglutinin I, conjugated to rhodamine, and lesion volume was determined by confocal microscopy and image analysis software. There was a minimum of six animals per group. **C**: Mice received 1 μL of intravitreal injection of 2 μg per eye siRNAs against IRE1α, ATF6, or CRYAB in the presence or absence of 5 ng VEGF164 neutralizing antibody at laser injury. Scrambled siRNA acted as a control. **D**: Mice received a 1-μL intravitreal injection of 5 μmol/L MG132 or 50 μmol/L AEBSF in the presence or absence of 5 ng of VEGF164 neutralizing antibody at laser injury. A 5 ng per eye vehicle and an Fc fragment were included as controls. **E** and **F**: Mouse pups underwent the OIR model, and animals were terminated at P17. There was a minimum of 12 animals per group. The average number of preretinal new-vessel nuclei was determined per section. **E**: Mouse pups received a 0.5-μL intravitreal injection of 1 μg per eye siRNA against IRE1α, ATF6, or CRYAB in the presence or absence of 5 ng VEGF164 neutralizing antibody at P12 (immediately after being removed from the hypoxic chamber). **F**: Mouse pups received a 0.5-μL intravitreal injection of 5 μmol/L MG132 or 50 μmol/L AEBSF in the presence or absence of 5 ng of VEGF164 neutralizing antibody at P12. A 5 ng per eye vehicle and the appropriate Fc fragment were included as controls. *$P < 0.05$ versus vehicle. Data are presented as means ± SEM. $^{\dagger}P < 0.05$ versus anti-VEGF; $^{\ddagger}P < 0.05$ versus scrambled siRNA without anti-VEGF; $^{\S}P < 0.05$ versus ATF6 siRNA; $^{\P}P < 0.05$ versus IRE1 siRNA; $^{\|}P < 0.05$ versus CRYAB siRNA.

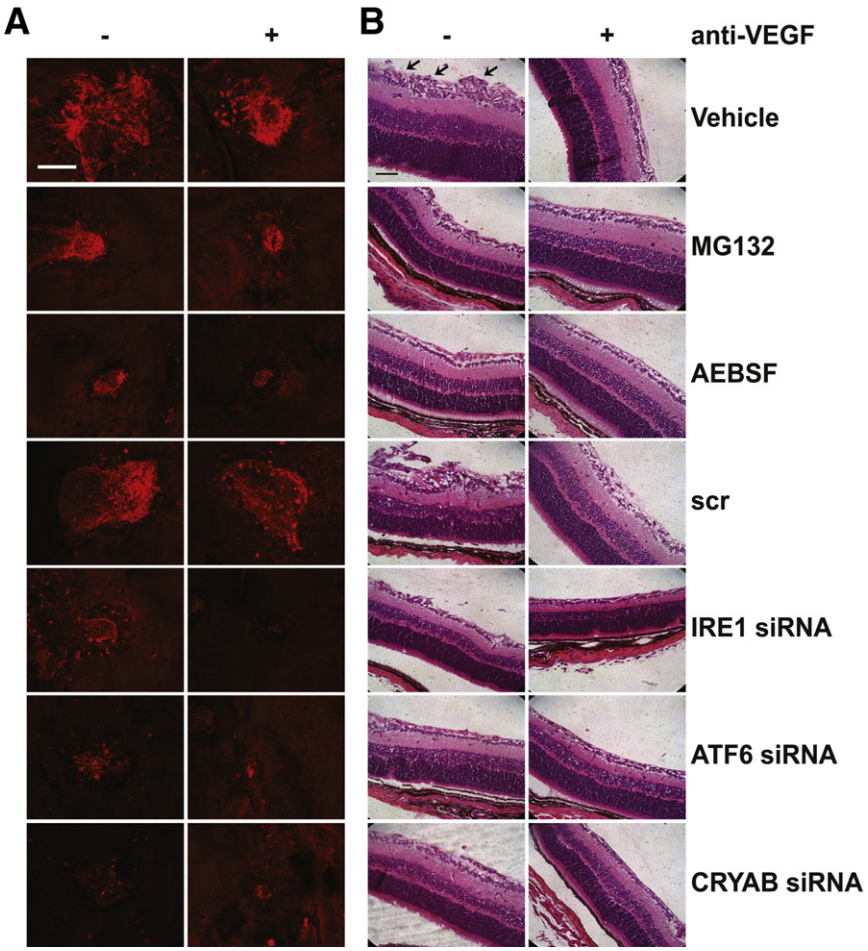

Figure 7 Representative photomicrographs showing the effect of UPR blockade and/or VEGF neutralization on vascular lesion formation in the CNV and OIR mouse models. **A**: Representative photomicrographs of the vascular lesion quantified in Figure 6, C and D. Mice underwent the CNV model, and animals were terminated at 14 days after laser injury. Lesions were labeled with vascular-specific dye, Ricinus Communis Agglutinin I, conjugated to rhodamine, and lesions were visualized by confocal microscopy. Mice received a 1-μL intravitreal injection of 2 μg per eye siRNAs against IRE1α, ATF6, or CRYAB, 5 μmol/L MG132, or 50 μmol/L AEBSF in the presence or absence of 5 ng VEGF164 neutralizing antibody at laser injury. Scrambled siRNA (scr) acted as a control. **B**: Representative photomicrographs of the vascular lesion quantified in Figure 6, E and F. Mouse pups underwent the OIR model, and animals were terminated at P17. Retinal sections were prepared and imaged. Mouse pups received a 0.5-μL intravitreal injection of 1 μg per eye siRNA against IRE1α, ATF6, CRYAB, 5 μmol/L MG132, or 50 μmol/L AEBSF in the presence or absence of 5 ng VEGF164 neutralizing antibody at P12 (immediately after being removed from the hypoxic chamber). Scale bar = 20 μm.

or transcriptional regulators, can protect proteins from proteosomal degradation and, thus, sustain their lifetime within a cell.[12] This appears to be the case for VEGF because activation of the UPR led to an increase in intracellular VEGF, and either siRNA or pharmacological inhibition of the IRE1α and ATF6 pathways promoted VEGF degradation and a major reduction in intracellular VEGF. Furthermore, Ghosh et al[13] have reported that CRYAB, in addition to VEGF, has interactive sequences for other angiogenic factors, such as fibroblast growth factor and insulin. Thus, CRYAB may act as a central regulator for several different intracellular signaling pathways.

We next demonstrated that knockdown of CRYAB or its upstream pathways elicited partial inhibition of VEGF-induced *in vitro* angiogenesis. A similar response was also observed in both the CNV and OIR mouse models of ocular neovascularization after intravitreal application of siRNA or pharmacological inhibitors of the UPR. Interestingly, siRNA knockdown of the UPR pathways generally elicited a greater inhibition than anti-VEGF neutralizing antibody (even at the highest concentration of antibody tested) in both *in vitro* and *in vivo* angiogenesis models. This may be, in part, due to the concentration of test compound used; however, the UPR can, through transcriptional control, regulate the expression of several growth factors, including VEGF.[11,36,37] Nevertheless, there is some debate as to which UPR pathways are involved, and this may be cell type specific.

Based on our observations, we hypothesized that activation of the UPR and subsequent CRYAB up-regulation may be critical in sustaining VEGF signaling, which may explain the limited success achieved in neutralizing only extracellular VEGF.[12] We, therefore, co-administered a VEGF neutralizing antibody with siRNA against UPR proteins or putative pharmacological inhibitors of the UPR in the OIR and CNV mouse models. Our studies confirmed our hypothesis that combination therapy to block both the intracellular and extracellular pathways would be more effective than either treatment on its own. Surprisingly, although CRYAB knockdown was additive with VEGF neutralizing antibody in both the OIR and CNV mouse models of neovascularization, different UPR pathways appeared to be involved, with IRE1α predominating in the CNV model and ATF6 in the OIR model. This would agree with the view that XBP1/IRE1α and ATF6 pathways operate in parallel and may interact with each other on ER stress.[10,30,38] However, regulation of the UPR signaling pathways is complex because IRE1α, XBP1, PERK, and ATF6 are themselves transcriptionally controlled by the UPR.[30]

We also tested two putative pharmacological inhibitors, MG132 and AEBSF, which we and others have shown can inhibit the IRE1α and ATF6 pathways of the UPR (Table 1). Both of these compounds were effective at inhibiting *in vitro* and *in vivo* angiogenesis and acted additively with VEGF neutralizing antibody to inhibit CNV, but not retinal neovascularization, in the OIR model, thus emphasizing their different pathogenic mechanisms. However, neither of these compounds is specific for the UPR pathways: MG132 is a commonly used proteasome inhibitor, and AEBSF is a serine protease/NADPH oxidase inhibitor. Both have previously been reported to inhibit angiogenesis, but the mechanism was not well characterized.[39,40] However, the efficacy of these compounds supports high-throughput screening to identify small molecules with specificity for proteins in the UPR for use in clinical studies. However, caution should prevail because blocking the UPR outright may be counterproductive because it facilitates cellular homeostasis and CRYAB may offer the best target.

It is tempting to ascribe the UPR-mediated accumulation of intracellular VEGF and sustained angiogenesis, even in the absence of extracellular VEGF, to an intracellular VEGF signaling pathway. An intracrine VEGF signaling pathway has been identified in several cell types, including vascular endothelial cells.[7,41,42] Inhibition of this intracellular pathway has been reported to promote endothelial cell apoptosis and cannot be rescued by exogenous VEGF.[7] This indicates that the intracrine VEGF signaling can play an important role in vascular aberrant neovascularization, as occurs in the retina and tumors, and that the intracrine pathway can operate independently of the classic extracellular VEGF pathway. However, little is known about how the intracrine pathway is regulated. Based on our observations, we postulate that activation of the UPR and subsequent CRYAB up-regulation may be critical in initiating the intracrine VEGF signaling pathway. It is, thus, possible that intracrine VEGF signaling acts as a primary intrinsic resistance to anti-VEGF therapies and that this may explain the limited success achieved in neutralizing only extracellular VEGF.[12] Our *in vitro* data provide some support for this, but it will be particularly challenging to confirm these results *in vivo*.

The impact of this study is extensive and far reaching, given that cancer is a major cause of morbidity in the population and neovascular diseases of the eye, including the exudative or wet form of AMD, diabetic retinopathy, and retinopathy of prematurity, represent the leading causes of vision impairment in developed countries. Blockade of extracellular VEGF with ranibizumab (Lucentis) or bevacizumab (Avastin) can significantly reduce ocular angiogenesis, but unfortunately, many patients are refractory and the inhibition of angiogenesis is not sustained.[2,3,6] Although reasonable success has been observed in the treatment of ocular angiogenesis, the outcomes in tumor angiogenesis have remained poor.[43] The challenge, therefore, is to find adjunct therapies. Our study supports that inhibition of UPR may obviate the need for as-frequent anti-VEGF injections and lower the dose of exogenous VEGF blocker needed to act synergistically to elicit complete regression of the vascular lesion. Our study sets a paradigm for the development of combination therapy to inhibit both the extracellular and UPR-mediated VEGF pathways in the fight against pathological angiogenesis.

References

1. Penn JS, Madan A, Caldwell RB, Bartoli M, Caldwell RW, Hartnett ME: Vascular endothelial growth factor in eye disease. Prog Retin Eye Res 2008, 27:331−371
2. Abouammoh M, Sharma S: Ranibizumab versus bevacizumab for the treatment of neovascular age-related macular degeneration. Curr Opin Ophthalmol 2011, 22:152−158
3. Chiang A, Regillo CD: Preferred therapies for neovascular age-related macular degeneration. Curr Opin Ophthalmol 2011, 22:199−204
4. Brown DM, Michels M, Kaiser PK, Heier JS, Sy JP, Ianchulev T; ANCHOR Study Group: Ranibizumab versus verteporfin photodynamic therapy for neovascular age-related macular degeneration: two-year results of the ANCHOR study. Ophthalmology 2009, 116:57−65.e5
5. Chang TS, Bressler NM, Fine JT, Dolan CM, Ward J, Klesert TR: Improved vision-related function after ranibizumab treatment of neovascular age-related macular degeneration: results of a randomized clinical trial. Arch Ophthalmol 2007, 125:1460−1469
6. Waisbourd M, Goldstein M, Loewenstein A: Treatment of diabetic retinopathy with anti-VEGF drugs. Acta Ophthalmol 2011, 89:203−207
7. Lee S, Chen TT, Barber CL, Jordan MC, Murdock J, Desai S, Ferrara N, Nagy A, Roos KP, Iruela-Arispe ML: Autocrine VEGF signaling is required for vascular homeostasis. Cell 2007, 130:691−703
8. Gerber HP, Ferrara N: The role of VEGF in normal and neoplastic hematopoiesis. J Mol Med 2003, 81:20−31
9. Glembotski CC: The role of the unfolded protein response in the heart. J Mol Cell Cardiol 2008, 44:453−459
10. Malhotra JD, Kaufman RJ: The endoplasmic reticulum and the unfolded protein response. Semin Cell Dev Biol 2007, 18:716−731
11. Ghosh R, Lipson KL, Sargent KE, Mercurio AM, Hunt JS, Ron D, Urano F: Transcriptional regulation of VEGF-A by the unfolded protein response pathway. PLoS One 2010, 5:e9575
12. Ruan Q, Han S, Jiang WG, Boulton ME, Chen ZJ, Law BK, Cai J: alphaB-crystallin, an effector of unfolded protein response, confers anti-VEGF resistance to breast cancer via maintenance of intracrine VEGF in endothelial cells. Mol Cancer Res 2011, 9:1632−1643
13. Ghosh JG, Shenoy AK Jr, Clark JI: Interactions between important regulatory proteins and human alphaB crystallin. Biochemistry 2007, 46:6308−6317
14. Kase S, He S, Sonoda S, Kitamura M, Spee C, Wawrousek E, Ryan SJ, Kannan R, Hinton DR: alphaB-crystallin regulation of angiogenesis by modulation of VEGF. Blood 2010, 115:3398−3406
15. Dimberg A, Rylova S, Dieterich LC, Olsson AK, Schiller P, Wikner C, Bohman S, Botling J, Lukinius A, Wawrousek EF, Claesson-Welsh L: alphaB-crystallin promotes tumor angiogenesis by increasing vascular survival during tube morphogenesis. Blood 2008, 111:2015−2023
16. Cai J, Jiang WG, Grant MB, Boulton M: Pigment epithelium-derived factor inhibits angiogenesis via regulated intracellular proteolysis of vascular endothelial growth factor receptor 1. J Biol Chem 2006, 281:3604−3613
17. Zhao B, Cai J, Boulton M: Expression of placenta growth factor is regulated by both VEGF and hyperglycaemia via VEGFR-2. Microvasc Res 2004, 68:239−246
18. Cai J, Chen Z, Ruan Q, Han S, Liu L, Qi X, Boye SL, Hauswirth WW, Grant MB, Boulton ME: γ-Secretase and presenilin mediate cleavage and phosphorylation of vascular endothelial growth factor receptor-1. J Biol Chem 2011, 286:42514−42523
19. Lauer G, Sollberg S, Cole M, Krieg T, Eming SA: Generation of a novel proteolysis resistant vascular endothelial growth factor165

variant by a site-directed mutation at the plasmin sensitive cleavage site. FEBS Lett 2002, 531:309−313
20. Caballero S, Sengupta N, Afzal A, Chang KH, Li Calzi S, Guberski DL, Kern TS, Grant MB: Ischemic vascular damage can be repaired by healthy, but not diabetic, endothelial progenitor cells. Diabetes 2007, 56:960−967
21. Qi X, Cai J, Ruan Q, Liu L, Boye SL, Chen Z, Hauswirth WW, Ryals RC, Shaw L, Caballero S, Grant MB, Boulton ME: Presenilin-1 Inhibition of Murine Choroidal neovascularization is Associated with Reduction of Superoxide and Proinflammatory Cytokines. Invest Ophthalmol Vis Sci 2012, 53:574−585
22. Kleinman ME, Yamada K, Takeda A, Chandrasekaran V, Nozaki M, Baffi JZ, Albuquerque RJ, Yamasaki S, Itaya M, Pan Y, Appukuttan B, Gibbs D, Yang Z, Kariko K, Ambati BK, Wilgus TA, DiPietro LA, Sakurai E, Zhang K, Smith JR, Taylor EW, Ambati J: Sequence- and target-independent angiogenesis suppression by siRNA via TLR3. Nature 2008, 452:591−597
23. Lee AH, Iwakoshi NN, Anderson KC, Glimcher LH: Proteasome inhibitors disrupt the unfolded protein response in myeloma cells. Proc Natl Acad Sci U S A 2003, 100:9946−9951
24. Okada T, Haze K, Nadanaka S, Yoshida H, Seidah NG, Hirano Y, Sato R, Negishi M, Mori K: A serine protease inhibitor prevents endoplasmic reticulum stress-induced cleavage but not transport of the membrane-bound transcription factor ATF6. J Biol Chem 2003, 278:31024−31032
25. Healy SJ, Gorman AM, Mousavi-Shafaei P, Gupta S, Samali A: Targeting the endoplasmic reticulum-stress response as an anticancer strategy. Eur J Pharmacol 2009, 625:234−246
26. Hu WK, Liu R, Pei H, Li B: Endoplasmic reticulum stress-related factors protect against diabetic retinopathy. Exp Diabetes Res 2012, 2012:507986
27. Li J, Wang JJ, Yu Q, Wang M, Zhang SX: Endoplasmic reticulum stress is implicated in retinal inflammation and diabetic retinopathy. FEBS Lett 2009, 583:1521−1527
28. Li X, Zhang K, Li Z: Unfolded protein response in cancer: the physician's perspective. J Hematol Oncol 2011, 4:8
29. Salminen A, Kauppinen A, Hyttinen JM, Toropainen E, Kaarniranta K: Endoplasmic reticulum stress in age-related macular degeneration: trigger for neovascularization. Mol Med 2010, 16:535−542
30. Walter P, Ron D: The unfolded protein response: from stress pathway to homeostatic regulation. Science 2011, 334:1081−1086
31. Hetz C: The unfolded protein response: controlling cell fate decisions under ER stress and beyond. Nat Rev Mol Cell Biol 2012, 13: 89−102
32. Pawlowska Z, Baranska P, Jerczynska H, Koziolkiewicz W, Cierniewski CS: Heat shock proteins and other components of cellular machinery for protein synthesis are up-regulated in vascular endothelial cell growth factor-activated human endothelial cells. Proteomics 2005, 5:1217−1227
33. Carver JA, Lindner RA: NMR spectroscopy of alpha-crystallin: insights into the structure, interactions and chaperone action of small heat-shock proteins. Int J Biol Macromol 1998, 22:197−209
34. De S, Rabin DM, Salero E, Lederman PL, Temple S, Stern JH: Human retinal pigment epithelium cell changes and expression of alphaB-crystallin: a biomarker for retinal pigment epithelium cell change in age-related macular degeneration. Arch Ophthalmol 2007, 125: 641−645
35. Dong Z, Kase S, Ando R, Fukuhara J, Saito W, Kanda A, Murata M, Noda K, Ishida S: Alphab-crystallin expression in epiretinal membrane of human proliferative diabetic retinopathy. Retina 2012, 32: 1190−1196
36. Bouvier N, Fougeray S, Beaune P, Thervet E, Pallet N: The unfolded protein response regulates an angiogenic response by the kidney epithelium during ischemic stress. J Biol Chem 2012, 287:14557−14568
37. Pereira ER, Liao N, Neale GA, Hendershot LM: Transcriptional and post-transcriptional regulation of proangiogenic factors by the unfolded protein response. PLoS One 2010, 5(pii):e12521
38. Chakrabarti A, Chen AW, Varner JD: A review of the mammalian unfolded protein response. Biotechnol Bioeng 2011, 108:2777−2793
39. Matsuo Y, Sawai H, Ochi N, Yasuda A, Sakamoto M, Takahashi H, Funahashi H, Takeyama H, Guha S: Proteasome inhibitor MG132 inhibits angiogenesis in pancreatic cancer by blocking NF-kappaB activity. Dig Dis Sci 2010, 55:1167−1176
40. Polytarchou C, Papadimitriou E: Antioxidants inhibit angiogenesis in vivo through down-regulation of nitric oxide synthase expression and activity. Free Radic Res 2004, 38:501−508
41. Browder TM, Abrams JS, Wong PM, Nienhuis AW: Mechanism of autocrine stimulation in hematopoietic cells producing interleukin-3 after retrovirus-mediated gene transfer. Mol Cell Biol 1989, 9: 204−213
42. Gerber HP, Malik AK, Solar GP, Sherman D, Liang XH, Meng G, Hong K, Marsters JC, Ferrara N: VEGF regulates haematopoietic stem cell survival by an internal autocrine loop mechanism. Nature 2002, 417:954−958
43. Cai J, Han S, Qing R, Liao D, Law B, Boulton ME: In pursuit of new anti-angiogenic therapies for cancer treatment. Front Biosci 2011, 16: 803−814